Corrosion Engineering, Science and Technology, Volume 46, Number 4, June 2011 , pp. 318-329

PREFERENTIAL WELD CORROSION OF X65 PIPELINE STEEL IN FLOWING BRINES CONTAINING CARBON DIOXIDE

K.Alawadhi[+] & M.J.Robinson
School of Applied Sciences
Cranfield University
Bedford MK43 0AL, UK

[+] present address; Kuwait College of Technological Studies

ABSTRACT

The aim of this research was to investigate the cause of the severe localised corrosion that sometimes occurs at welds in carbon steel pipelines carrying hydrocarbons and inhibited brines saturated with carbon dioxide. A rotating cylinder electrode (RCE) apparatus was designed so that electrodes machined from the weld metal, heat affected zone (HAZ) and parent material of welded X65 pipeline steel could be galvanically coupled and tested in high shear stress conditions. The galvanic currents flowing between the weld regions were recorded using zero-resistance ammeters and their self-corrosion rates were found by polarisation resistance measurements. The total corrosion rate of each weld region was obtained from the sum of the self-corrosion and galvanic contributions.

In uninhibited conditions, the weld metal and HAZ were both cathodic to the parent material and localised corrosion was prevented. However, when an oilfield corrosion inhibitor was present a current reversal took place, which resulted in accelerated weld corrosion. Electrochemical impedance spectroscopy (EIS) showed that the inhibitor film had lower electrical resistance and was less protective on the weld metal than on the parent material. At the highest shear stress, a second current reversal could occur when the inhibitor was removed from all regions of the weld and there was a return to the original galvanic behaviour. It was concluded that preferential weld corrosion was caused by unstable conditions in which the inhibitor film was selectively disrupted on the weld metal but remained effective on the other weld regions.

Keywords: weld corrosion, carbon steel, inhibitor, carbon dioxide

INTRODUCTION

It is well known that galvanic corrosion can occur between the different regions of a weld due to differences in composition and microstructure. If the weld metal and heat affected zone are anodic to the parent material then localised metal loss can take place in those regions [(1)]. An example of severe preferential weld corrosion (PWC) in a pipeline containing hydrocarbons and brine saturated with carbon dioxide [(2)] is shown in Figure 1. This problem is accentuated by the small surface areas of the weld metal and heat-affected zones compared to the large area of the parent pipe material. In contrast, if the weld metal is selected to be slightly noble to the

parent material then it will remain cathodic and this can be expected to reduce galvanic corrosion of the weld metal and distribute it instead over the large area of the parent material. In practice, additions of Ni and Cr are often made to the weld metal to increase its strength and these have the further effect of providing a more noble potential [3]. Galvanic corrosion is not the only consideration in weld corrosion, however, and even cathodic weld metals containing 1%Ni have been reported to display preferential metal loss due to a high rate of self-corrosion [3].

The microstructure is another factor that influences the corrosion behaviour. For example, the heat affected zone has the same composition as the parent material but its modified microstructure can lead to accelerated corrosion. It has been shown that preferential weld corrosion in carbon steels is accelerated by increasing the hardness, the grain size and the proportion of aligned second phase in the weld metal [4]. Matching weld consumables, with the same composition as the parent material, have been shown to give the best resistance to PWC, whereas both 1%Ni and 1% Si additions are detrimental.

Recent research has shown that it is more difficult to inhibit corrosion of high nickel-containing weld metals [5]. In some cases, addition of an inhibitor caused a reversal of the galvanic current and this would appear to explain the reported incidence of preferential weld corrosion when those weld consumables had been used.

Weld corrosion has been investigated by a range of experimental techniques. Mini-electrochemical cells have been used carry out polarisation measurements across the different regions of the weld [6,7]. Other studies [8] have employed scanning voltage electrode techniques (SVET) and localised electrochemical impedance spectroscopy (LEIS). Galvanic current measurements have generally been achieved by sectioning the weld to produce individual electrodes of weld metal, heat affected zone and parent material, attaching wires to carry the currents and assembling them in resin, prior to exposing them to the corrosive conditions [2-5,9]. The flow rate of the electrolyte is an important factor in CO_2 corrosion and in some studies the hydrodynamic conditions have been controlled using a flow channel [10], a re-circulating flow loop [5] and rotating cylinder electrodes [2,9].

The aim of the work described in this paper was to investigate the conditions under which galvanic current reversal takes place and to explain why the addition of a corrosion inhibitor appears to cause these changes. A novel rotating cylinder electrode was designed to operate at speeds up to 5000 rpm and record galvanic current measurements under hydrodynamic conditions representative of flow in a pipe. In addition, the self-corrosion rates of the different regions of the weld were measured by separating each electrode in turn and performing linear polarisation resistance (LPR) scans and electrochemical impedance spectroscopy (EIS).

EXPERIMENTAL

Welded pipeline steel

All tests were carried out on samples machined from welded X65 steel pipe with the composition shown in Table 1. The steel had been thermomechanically controlled rolled to give a 32mm thickness and a hardness of 200-210 Hv. The longitudinal

double-vee pipeline weld had been produced by the submerged arc process, with a relatively high heat input (5-10 J/mm) giving a hardness of 223-230 Hv. The composition of the weld metal is also given in Table 1 and was similar to that of the parent material, except for the addition of 0.68% Ni and smaller quantities of Cr and Mo. A sample was cut from the weld, polished and etched to identify the positions of the parent material, heat affected zones and weld metal, as shown in Figure 2. Micrographs of each region and a micro-hardness profile across the weld are shown in Figure 3. The microstructure of the parent material consisted of fine equiaxed ferrite with small amounts of pearlite. The fine-grained HAZ was similar in appearance, having slightly larger equiaxed ferrite and a small quantity of an aligned second phase. The coarse grained HAZ displayed acicular ferrite that had formed throughout the enlarged prior austenite grains. In the weld metal, primary ferrite had formed on prior austenite grain boundaries, with a finer aligned microstructure within the grains.

Rotating Cylinder Electrodes

Electrochemical corrosion rate measurements were carried out using a rotating cylinder electrode (RCE) produced from the different regions of the weld [11]. An advantage of using the rotating cylinder electrode is that the hydrodynamic conditions are very well defined and it is feasible to translate the conditions that are known to exist in a production pipeline to those used in laboratory tests [12,13]. However, there appears to have been little attempt to use this method for investigating weld corrosion due to the technical difficulties of making multiple electrical connections to rotating electrodes, consisting of three or more different regions of a weld.

The RCE consisted of hollow cylindrical samples, which were machined from each region of the weld (parent material, heat affected zone and weld metal) and had wires attached to carry the electrochemical signals. The three component parts were electrically isolated from each other by PTFE spacers, assembled onto an insulated shaft and secured with a retaining nut, as shown in Figure 4. The areas of the exposed parent material (PM), heat affected zone (HAZ) and weld metal (WM) were in the ratio 8:1:2 to represent the approximate proportions of each region in the vicinity of a typical pipeline weld. Clearly, in a pipeline there would be very large areas of parent material further from a weld but these are considered to have a lesser effect on localised corrosion due to the greater ionic path involved.

A set of high quality, multi-element slip rings were mounted on the motor driven shaft to take the electrical signals from the weld components to the electrochemical instrumentation. The slip rings had a maximum dynamic resistance of 10 milliohms so that electrical noise was very low and the assembly was rated for speeds of 13,000 rpm, well above the maximum of 5000 rpm used in this study.

The wall shear stress, τ_{RCE}, in the liquid at the rotating electrode surface was calculated from the following equation [14].

$$\tau_{RCE} = 0.079\, R_e^{-0.3}\, \rho\, r^2\, \omega^2 \qquad [1]$$

where R_e is Reynolds number for the flow, ρ is the liquid density, r is the radius of the RCE and ω is its angular velocity.

Electrochemical measurements

Galvanic currents The galvanic currents between each weld region were recorded every sixty seconds during the test using a multi-channel zero resistance ammeter (ACM Instruments GalvoGill 12) connected to a data logging PC. The currents from the parent material to the weld metal and from the HAZ to the weld metal were recorded on two channels and, as the three electrodes were in the short-circuit condition, their individual galvanic currents were established from the following relationship;-

$$I_{PM} + I_{HAZ} + I_{WM} = 0 \qquad [2]$$

Self-Corrosion Rates The self-corrosion rates of the three weld regions were measured by uncoupling each electrode of the RCE in turn and carrying out linear polarisation resistance measurements (LPR) using a platinum gauze secondary electrode, a standard calomel reference electrode and a Sycopel Electronics AW2 low noise potentiostat. The potential of each weld component was scanned 10 mV above and below its open circuit value, at a scan rate of 10 mV min^{-1}, and the current response was recorded. The polarisation resistance, R_p, was obtained from the best-fit gradient of the potential/current graph and the corrosion current, I_{CORR}, was then found from the equation;-

$$I_{CORR} = B / R_P \qquad [3]$$

where B is a constant for the material and its environment, taken as 13 mV [15]. Due to the very small potential perturbation applied, the polarisation resistance method can be repeated over long periods without changing the behaviour of the steel significantly from its freely corroding condition.

The total corrosion rates of the three weld regions were found from the sum of their self-corrosion rate and galvanic corrosion rate.

Electrochemical Impedance Spectroscopy (EIS) In addition to LPR measurements to record self-corrosion rates, EIS was used in some experiments to investigate the corrosion mechanism and identify components of the equivalent circuits describing the corroding metal surfaces. In particular, it was used to measure the resistance of surface films that resulted from either the corrosion process or the action of the inhibitor. The measurements were carried out using a Gill AC potentiostat from ACM Instruments with a 10mV signal ranging in frequency from 20 KHz to 5 mHz.

Experimental Conditions

The experiments were carried out at ambient temperature (20^{o}C) and at 50^{o}C and 70^{o}C in a cell containing artificial seawater, saturated with carbon dioxide. Particular care was taken in preparing the electrode surface before the test and in maintaining oxygen free conditions in the electrolyte as these were found to be important in obtaining reproducible results. In each test, the RCE was held stationary for the first ten hours, during which time a stable dark grey film developed on the electrode surfaces. The RCE was then rotated for 20 minutes at 500 rpm while one of the electrochemical techniques was employed. The measurements were repeated with the speed increased to 1000 rpm and then in steps of 1000 rpm up to 5000 rpm. In one experimental run, galvanic currents were recorded at 1 minute intervals while in others polarisation resistance measurements or EIS scans were carried out in the static condition and at each rotational speed. The experiments were generally repeated one or more times.

The same methodology was used to study the corrosion behaviour of each weld region in seawater in both the uninhibited condition and when containing CORRTREAT 05-193, an oilfield corrosion inhibitor supplied by Clariant Oil Services. The inhibitor consisted of a blend of neutralising amines and synergists in a water/glycol based solvent package. In each case, it was used at a concentration of 30 ppm by volume, which is typical of oilfield practice [(5)].

RESULTS AND DISCUSSION

Galvanic Current Measurements

Uninhibited Conditions The parent material and the HAZ were both anodic (+ve currents) to the weld metal at each test temperature. The results for the ambient temperature condition are given in Figure 5. The currents gradually decreased over the first 600 minutes due to the formation of the dark grey surface film, which appeared to be partially protective. Clearly, it was favourable for the weld metal to be the cathodic component in the couple as this condition ensured that its corrosion rate was reduced by sacrificial protection of the other weld regions. Typical open-circuit potentials of each weld region in uninhibited seawater at 5000 rpm, shown in Table 2, confirm that the weld metal was the most noble component of the couple at the three test temperatures. The potentials differed by only a few millivolts but this was a consistent and reproducible trend in each experiment.

Under fluid flow conditions, the galvanic currents increased approximately linearly with the rotational speed of the RCE. It could be seen from the visual appearance that the rotation caused partial removal of the film. It is significant that the currents shown in Figure 5 remained higher after the rotation period, when the film had been thinned or removed, than they had been immediately beforehand, again supporting the view that the film was partially protective.

Although the anodic current measured on the parent material was larger than that on the HAZ, when the different electrode areas were taken into consideration their

current densities were very similar. This is not surprising as they had the same elemental composition and differed only in their microstructures.

Inhibited Conditions The galvanic currents that resulted from the addition of 30 ppm of oilfield corrosion inhibitor displayed different behaviour to those in uninhibited seawater and the results obtained in ambient conditions are shown in Figure 6. During most of the pre-exposure period the parent material was again anodic to the weld metal but, as expected in inhibited conditions, the current was much reduced (20 μA for the initial value compared to 150 μA for the uninhibited case). The initial currents decreased rapidly over the first hour as an inhibitor film developed on the electrode surfaces.

When the electrode was rotated, the presence of the inhibitor caused a marked change in the galvanic corrosion behaviour. A rapid current reversal took place with the weld metal and HAZ both becoming anodic to the parent metal. The galvanic current was particularly high on the weld metal at the highest rotational speed, suggesting that the inhibitor film was more adversely affected by flow on this material than on the other weld regions. It is thought that the high shear stress caused preferential removal of the inhibitor film from the weld metal, leading to an active shift in its potential. This situation is undesirable and would be expected to result in localised weld corrosion of the type that has sometimes been reported to occur in service [(2)]. However, when the RCE rotation was stopped the galvanic currents decreased very rapidly to their previous level, suggesting that complete film removal had not occurred.

In some tests at the highest rotational speed, a second current reversal took place, with the weld metal returning suddenly to the cathodic behaviour that it had displayed in the uninhibited conditions. An example of this situation is shown in Figure 7. It appears that the second current reversal occurred as the result of a change from the inhibitor film being disrupted preferentially on the weld metal to it being removed from all regions of the weld. In consequence, the ranking of the open-circuit potentials of the different weld regions reflected their behaviour in the uninhibited conditions, with the weld metal being the most cathodic. The small differences in the open-circuit potentials in inhibited conditions at 5000 rpm in Table 2 show the weld metal to be the most noble component and it is assumed that in these high shear stress experiments complete film removal had taken place.

Self-corrosion rates

Uninhibited conditions The self-corrosion rates, measured by LPR, displayed a steady increase over the range of rotational speeds. At ambient temperature, the rates were similar for the three weld regions and approximately doubled from stationary conditions (0.6 mm/y) to the highest flow rate at 5000 rpm (1.2 mm/y). At 50^{o}C and 70^{o}C there was a smaller increase with flow rate (close to 50%) but the corrosion rates of the weld metal exceeded those of the parent material and HAZ (by about 30% at 50^{o}C and more than 100% at 70^{o}C). The self-corrosion rates measured at 5000 rpm are summarized in Figures 9 and 11.

Inhibited conditions At ambient temperature the addition of the inhibitor reduced the self-corrosion rates to approximately 1% of their previous values and at 50^{o}C and

70°C the rates were still only 3% of the uninhibited levels. Figure 8 shows that Increasing the rotational speed of the RCE had little effect until 3000 – 4000 rpm (shear stress of 30 - 48 Nm^{-2}) when, unlike the uninhibited case, there was a marked increase in corrosion rate, which suggests that the inhibitor was being detached. At ambient temperature and 50°C the highest rate occurred on the HAZ but at 70°C the weld metal was greatest. The parent metal had the lowest self-corrosion rate in the inhibited solution at all temperatures.

In addition to having the highest self-corrosion rates, the HAZ and weld metal had been the anodes in the galvanic corrosion tests in inhibited conditions. However, as ranking the order of corrosion rates in the three weld regions differed with temperature it is unlikely that microstructural differences alone are the explanation. Rather, it appears that the cause was differences in surface protection related to inhibitor film formation, with poorer film properties occurring on the weld metal and HAZ than on the parent material.

Total corrosion rates

Uninhibited conditions The total corrosion rate of each weld region can be considered to be the sum of its self-corrosion and galvanic corrosion rates. The values at 5000 rpm in uninhibited conditions for the three test temperatures are compared in Figures 9 and 10. The overall pattern of behaviour of the weld corrosion was very consistent at each temperature but showed an increase in rate as the temperature was raised above ambient.

On all regions of the weld, the galvanic contribution was much smaller than the self-corrosion rate. This is not surprising as carbon-manganese steel is inherently susceptible to high self-corrosion rates in carbonic acid, whereas the small compositional and microstructural differences between the weld regions would not be expected to cause large galvanic currents.

Significantly, the cathodic galvanic current on the weld metal reduced its total corrosion rate so that it was the lowest of the three weld regions at ambient and 50°C, although it remained the highest at 70°C. In effect, the weld metal was partially protected by sacrificial corrosion of the parent material and the HAZ. It is interesting to note that the weld metal had the highest self-corrosion rates at 50°C and 70°C yet it also had the most noble potential, as it was the most cathodic in the galvanic current measurements. Clearly, the three weld regions had differences in both microstructure and chemical composition and these are likely to have affected the self-corrosion rates and galvanic currents in different ways.

Inhibited conditions The total corrosion rates at the three test temperatures are compared in Figures 11 and 12. Unlike the uninhibited case, the galvanic contribution was large in comparison to the self-corrosion rate, particularly at 70°C. Due to the cathodic behaviour of the parent material, following current reversal, its total corrosion current was negative, meaning that it would be fully protected from corrosion in the area adjacent to the weld. Note that at greater distances from the weld in a pipeline, the galvanic contribution would be smaller and some corrosion of the parent material would be expected.

The high anodic galvanic current on the weld metal was the main factor in it having the highest total corrosion rate at 70^{o}C. (The galvanic component was more than three times the self-corrosion rate). This behaviour, shown in Figures 11(c) and 12, appears to explain the incidence of preferential weld corrosion of pipelines in inhibited conditions that is sometimes reported to occur in service, as this temperature and flow rate represent typical pipeline operating conditions. The total corrosion rate is not as high as would occur in the absence of an inhibitor (Figures 9(c) and 10) but it is much more localised, occurring only on the weld metal and HAZ, and the rate of approximately 1mm/yr for the weld metal is sufficient to have been the cause of these cases.

The observation of increased galvanic currents between the weld regions at the high flow rates and at higher temperatures, in a way that did not occur at low flow rates and ambient temperature, strongly supports the view that these galvanic effects are brought about by differences in the formation and attachment of inhibitor films on each weld region. It is further evidence that a less protective film was formed on the weld metal and HAZ than on the parent material and, in consequence, this behaviour would have contributed to severe localised corrosion of the weld.

Clearly, in circumstances when a second current reversal took place and the inhibitor film was detached from all regions of the weld, localised weld corrosion would not be expected to occur. Therefore, preferential weld corrosion can be regarded as the result of unstable conditions in which only partial inhibitor film removal occurs. It was to investigate the properties of the inhibitor films that electrochemical impedance spectroscopy was carried out.

Electrochemical Impedance Spectroscopy (EIS)

Uninhibited conditions Figure 13 shows the Nyquist plot obtained for the parent material upon initial immersion in uninhibited solution under static conditions at ambient temperature and consists of a single depressed semicircle. The high frequency end of the plot intersected the x-axis near the origin as the solution resistance of the seawater was very low (approximately 10 ohms). The charge transfer resistance, obtained from the difference between the two points of intersection, was close to 550 ohms cm^{2}, corresponding to a corrosion rate of approximately 0.27 mm/y.

After 10 hours immersion under static conditions, during which time a dark grey film formed on the surface, the plot changed to that shown in Figure 14. It again consisted of a single depressed semicircle, well defined at high frequency, but there was some influence of diffusion control at low frequency, as shown by the ‘tail’ in the last few data points. The charge transfer resistance had increased to 770 ohms cm^{2}, suggesting that the corrosion rate had been lowered slightly by the presence of the film.

Inhibited conditions Figure 15 shows the Nyquist plot for parent material under inhibited conditions at 50^{o}C, again after 10 hours exposure and with the RCE rotated at 5000 rpm to give the most severe flow conditions. The plot was distinctly different

from those obtained in uninhibited conditions, with the partial appearance of a second semicircle at high frequencies. Whereas the resistance and capacitance of the dark grey corrosion product film, which formed without the inhibitor, was insufficient to affect the Nyquist plot, the more protective nature of the inhibitor film produced a second semicircle, although it was partially merged with the main semicircle associated with charge transfer resistance, rather than being fully resolved [16]. The high frequency semicircle is shown at higher magnification on Figure 14 plot B and a curve fit suggests the resistance of the inhibitor film on the parent material at 50°C to have been close to 4200 ohms cm^2. The corresponding plot obtained at 70°C is shown in Figure 16 in which the inhibitor film was still in evidence but its resistance had decreased to approximately 1500 ohms cm^2.

The inhibitor film resistance was measured from the Nyquist plots for each weld region at both 50°C and 70°C and the results are compared in Figure 17. It is clear that the inhibitor film that formed on the parent material was of higher electrical resistance and therefore more protective than that on the weld metal and HAZ. These differences appear to offer a feasible explanation for the high rates of self-corrosion observed on these two weld regions.

Comparison between EIS and LPR results

It should be noted that EIS measurements are closely related to those obtained by LPR. At the scan rate of 10 mV/min used in this study each LPR measurement was equivalent to a single impedance measurement at a frequency of 4 mHz. The measured polarisation resistance was therefore a combination of solution resistance, film resistance and a contribution, if not all, of the charge transfer resistance. Therefore, with these limitations in mind, the EIS and the LPR results can both be regarded as a measure of the self-corrosion rate of each weld region.

It was shown that the weld metal and HAZ, which had the highest rates of self-corrosion and total corrosion, formed inhibitor films with low resistance, compared to that on the parent material. The charge transfer resistances on these weld regions were also lower than on the parent material, confirming the higher rates of self-corrosion.

Role of corrosion product films

The dark grey film that formed on the RCE under uninhibited conditions was examined by x-ray diffraction and shown to consist predominantly of Fe_3C, with smaller quantities of $FeCO_3$. In each region of the weld, the microstructure of the low carbon steel consisted of ferrite and iron carbides and the corrosion that had taken place in the carbonic acid had selectively removed the ferrite phase, leaving a network of iron carbide. As a result, the film had an open, porous structure, as shown in Figure 18, which explains why it offered little corrosion protection. In order for $FeCO_3$ films to form on the surface, it is necessary for sufficient Fe^{2+} ions to be present in the solution. Videm [17] found that at 70°C, 50 ppm of Fe^{2+} were required to produce a protective corrosion product film that would reduce the corrosion rate of carbon steels from 5 mm/y to 2 mm/y. However, in the present study it was shown from mass balance calculations that the Fe^{2+} ion concentration reached only 2.8 ppm

at the end of the experiments and this is thought to be the reason that protective sulphide films did not form [18]. Where such films do occur, the operating temperature is an important factor, as the stability and protectiveness of the films has been shown to increase at temperatures above 60°C [19].

The importance of surface films in enhancing preferential weld corrosion under inhibited conditions has been reported by other researchers [20]. Pre-corrosion, prior to addition of the inhibitor, appeared to hinder mass transfer to the metal surface, reducing inhibitor efficiency and extending the time for it to become effective. The alloy content of the steel is also thought to affect the composition of the films that form, both in freely corroding and inhibited conditions. The addition of 1%Ni to the weld metal has been widely used to overcome localised corrosion of welds in water injection systems, as well as improving strength and toughness. However, 1%Ni additions have been shown to accentuate the problem of preferential weld corrosion in CO_2 containing brines [21]. While metallurgical control of the welding procedure can be used to limit the extent of preferential weld corrosion, no weld metal composition was found to be completely immune from this form of attack.

Although the above factors may have an important influence, the work described in the present study has shown that the preferential weld corrosion was caused not by disparities in the properties of the corrosion product films but by the different protectiveness of the inhibitor films that formed on each region of the weld.

CONCLUSIONS

[1] In uninhibited conditions the weld metal was cathodic to the parent material and HAZ. This reduced the total corrosion rate of the weld metal as it was partially protected by the sacrificial corrosion of the other two weld regions.

[2] The addition of an oilfield corrosion inhibitor caused a current reversal at high flow rates. The inhibitor film was removed preferentially from the weld metal, so that it became strongly anodic and lead to a condition that would result in severe localised weld corrosion.

[3] In some cases, under high shear stress conditions, removal of the inhibitor film took place on all weld regions and a second current reversal occurred, with the weld metal again becoming the most noble weld component. It appears that preferential weld corrosion is caused by unstable conditions in which the inhibitor film is selectively disrupted on the weld metal but remains effective on the other weld regions.

[3] The total corrosion rates of each weld region could be considered in terms of their separate galvanic and self-corrosion components. In the absence of an inhibitor, the corrosion rates were dominated by the self-corrosion behaviour, whereas the presence of the inhibitor increased the galvanic contribution, particularly on the weld metal.

[4] Localised corrosion was shown to be most severe in inhibited conditions at 70°C and high flow rates, which is typical of conditions found in oil and gas pipelines. The

high shear stress reduced inhibitor coverage and EIS measurements showed that the inhibitor films had lower electrical resistance and were less protective on the weld metal and HAZ than on the parent material

Acknowledgement
The research described in this paper was supported by Clariant Oil Services.

REFERENCES

[1] C.Avendano-Castro, R.Galvan-Martinez, A.Contreras, M.Salazar, R.Orozco-Cruz, E.Martinez & R.Torres-Sanchez, Corrosion kinetics of pipeline carbon steel weld in aqueous solution containing H_2S, Corrosion Engineering, Science and Technology, Vol 44, No 2, pp 149-156 2009.

[2] G.I.Winning, N.Bretherton, A.McMahon & D.McNaughtan, Evaluation of weld corrosion behaviour and the application of corrosion inhibitors and combined scale/corrosion inhibitors, NACE Corrosion 2004, New Orleans, 28 March – 1 April 2004.

[3] S.Turgoose, J.W.Palmer & G.E.Dicken, Preferential weld corrosion of 1% Ni welds: effect of solution conductivity and corrosion inhibitors, Corrosion 2005, Paper 05275, (Houston, Texas: NACE International, 2005).

[4] C-M.Lee, S.Bond & P.Woollin, Preferential weld corrosion: effects of weldment microstructure and composition, Corrosion 2005, Paper 05277, (Houston, Texas: NACE International, 2005).

[5] E.Gulbrandsen & A.Dugstad, Corrosion loop studies of preferential weld corrosion and its inhibition in CO_2 environments, Corrosion 2005, Paper 05276, (Houston, Texas: NACE International, 2005).

[6] F.Martin, C.Garcia, P.Tiedra, Y.Blanco & M.Lopez, Application of minielectrochemical cell to corrosion studies of welded joints of austenitic stainless steel, Corrosion Engineering Science and Technology, Vol 43, No 4, pp 343-352, 2008.

[7] G.Garcia, M.P.de Tiedra, Y.Blanco, O.Martin & F.Martin, Intergranular corrosion of welded joints of austenitic stainless steels studied by using an electrochemical minicell, Corrosion Science, 50, 2390-2397, 2008.

[8] G.A.Zhang & Y.F.Cheng, Micro-electrochemical characterization of corrosion of welded X70 pipeline steel in near-neutral pH solution, Corrosion Science, 51, 1714-1724, 2009.

[9] A.Chalmers, I.G.Winning, D.McNaughtan & S.McNeil, Laboratory development of a corrosion inhibitor for a north sea main line offering enhanced environmental properties and weld corrosion protection, Corrosion 2006, Paper 06487, (Houston, Texas: NACE International, 2006).

[10] K.Fushimi, A.Naganuma, K.Azumi & Y.Kawahara, Current distribution during galvanic corrosion of carbon steel welded with type-309 stainless steel in NaCl solution, Corrosion Science, 50, 903-911, 2008.

[11] K.Alawadhi, M.Robinson, A.Chalmers & G.Winning, Inhibition of weld corrosion in flowing brines containing carbon dioxide, Corrosion 2008, Paper 08622, New Orleans, March 16-20, 2008, (Houston, Texas: NACE International, 2008).

[12] M.Bilson & K.Bremhorst, Comparison of turbulent scalar transport in a pipe and a rotating cylinder, Third International Conference on CFD in the Minerals and Process Industries, CSIRO, Melbourne, Australia, 10-12 December 2003.

[13] D.R.Gabe, G.D.Wilcox, J.Gonzalez-Garcia & F.C.Walsh, The rotating cylinder electrode: its continued development and application, J.Applied Electrochemistry 28, 759-780 (1998).

[14] D.C.Silverman, Rotating cylinder electrode – geometry relationships for prediction of velocity-sensitive corrosion, Corrosion, 44, 42 (1988).

[15] S.Nesic, J.Postlethwaite & S.Olsen, An electrochemical model for prediction of corrosion of mild steel in aqueous carbon dioxide solutions, Corrosion, 52, 280-294 (1996).

[16] G.W.Walter, A review of impedance plot methods used for corrosion performance analysis of painted metals, Corrosion Science, Vol 26, 9, 681-703 (1986).

[17] K.Videm, The influence of pH and concentration of bicarbonate and ferrous ions on the CO_2 corrosion of carbon steels, NACE Corrosion'93, Houston, Texas, paper 83 (1993).

[18] J.L.Mora-Mendoza & S.Turgoose, Fe_3C influence on the corrosion rate of mild steel in aqueous CO_2 systems under turbulent flow conditions, Corrosion Science, 44, 1223-1246 (2002).

[19] O.A.Nafday & S.Nesic, Iron carbonate scale formation and CO_2 corrosion in the presence of acetic acid, NACE Corrosion 2005, paper 05295 (2005).

[20] D.McNaughtan & I.G.Winning, Comparison of segmented weld corrosion tests with short and long pre-corrosion and the influence of synergist in corrosion inhibitors, 1st International Symposium on Oilfield Corrosion, Aberdeen, UK, 28 May 2004, paper 87553.

[21] D.Queen, Chi-Ming Lee & J.Palmer, Guidelines for the prevention, control and monitoring of preferential weld corrosion of ferritic steels in wet hydrocarbon production systems containing CO_2, 1st International Symposium on Oilfield Corrosion, Aberdeen, UK, 28 May 2004, paper 87552.

	C	Mn	Ni	Cr	Mo	Si	Al	Cu	V	P	S
Pipe	**0.08**	**1.6**	**0.04**	**0.02**	**0.01**	**0.3**	**0.04**	**0.02**	**0.05**	**0.009**	**0.0005**
Weld	**0.08**	**1.4**	**0.68**	**0.03**	**0.33**	**0.3**	**0.03**	**0.02**	**0.04**	**0.01**	**-**

Table 1. Compositions of X65 pipeline steel and weld metal (Wt%)

		Ecorr mV(SCE)		
		PM	WM	HAZ
Room Temp	Uninhibited	-721	-716	-721
	Inhibited	-688	-684	-700
50°C	Uninhibited	-723	-716	-723
	Inhibited	-679	-676	-672
70°C	Uninhibited	-726	-720	-729
	Inhibited	-684	-669	-677

Table 2. Comparison of open circuit potentials for each weld region in uninhibited and inhibited conditions at a rotational speed of 5000 rpm for parent material (PM), weld metal (WM) and heat affected zone (HAZ)

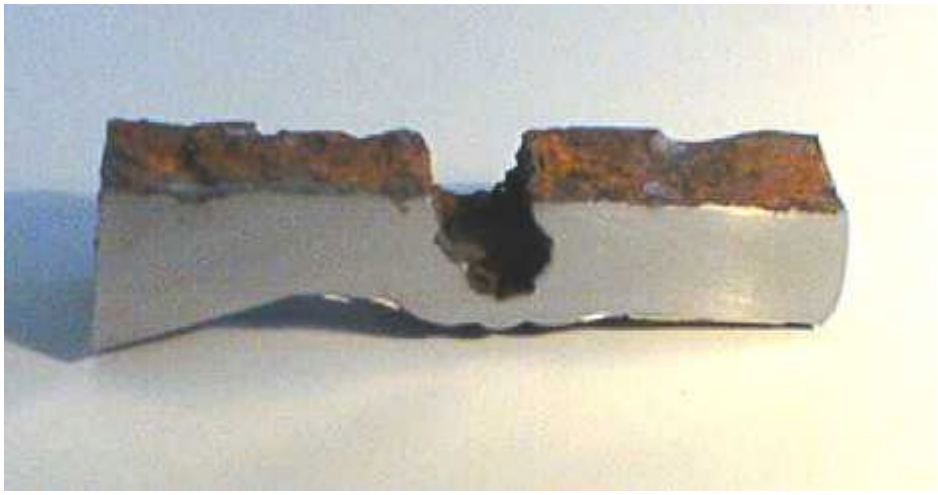

Figure 1 **An example of severe preferential weld corrosion in a carbon steel pipeline carrying inhibited oil and gas [(1)]**

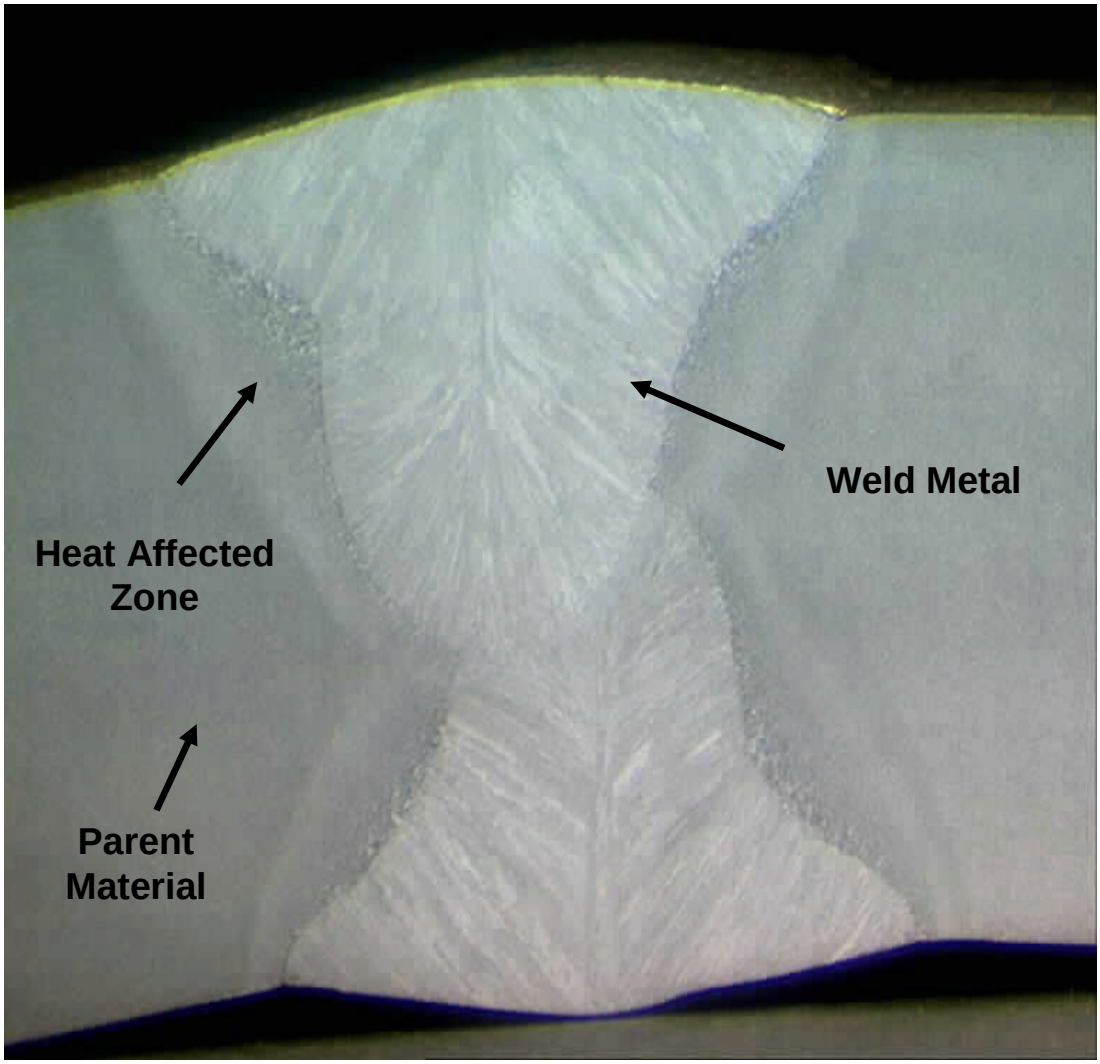

Figure 2 **Section of the weld in X65 pipeline steel showing the parent material, weld metal and heat affected zone**

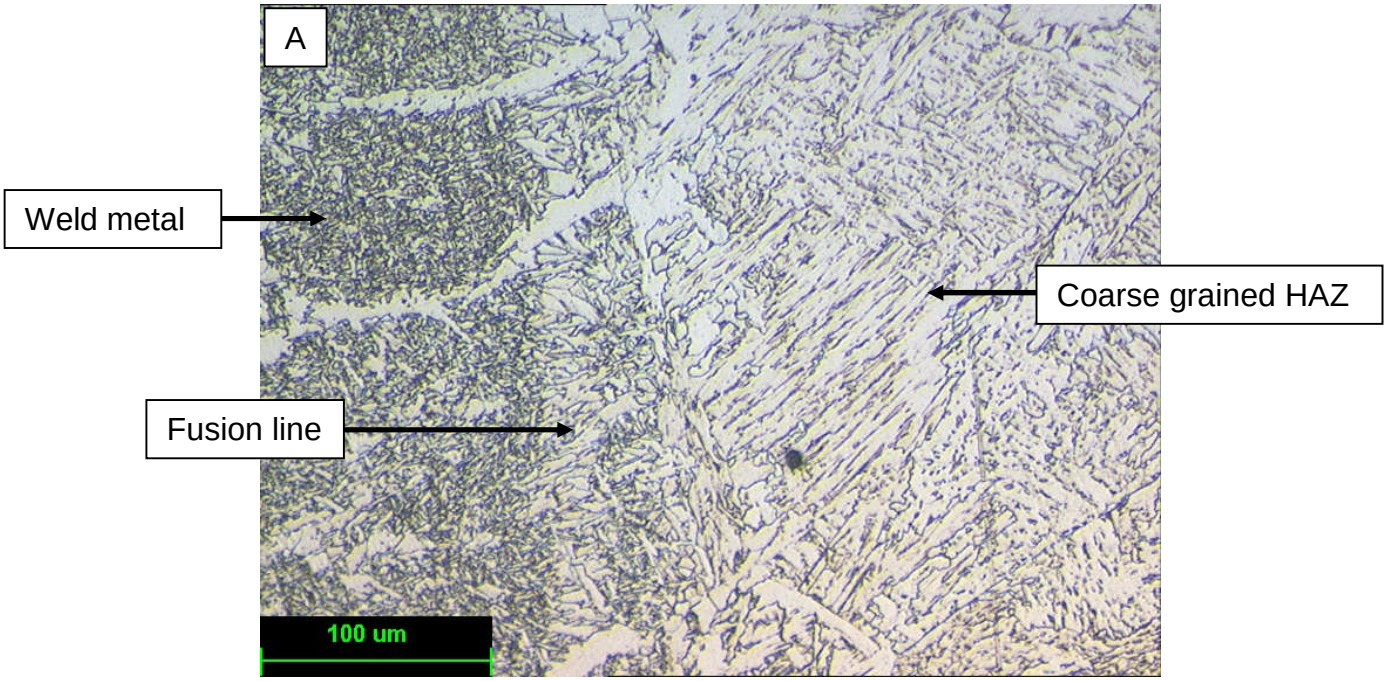
A
Weld metal
Coarse grained HAZ
Fusion line
100 um

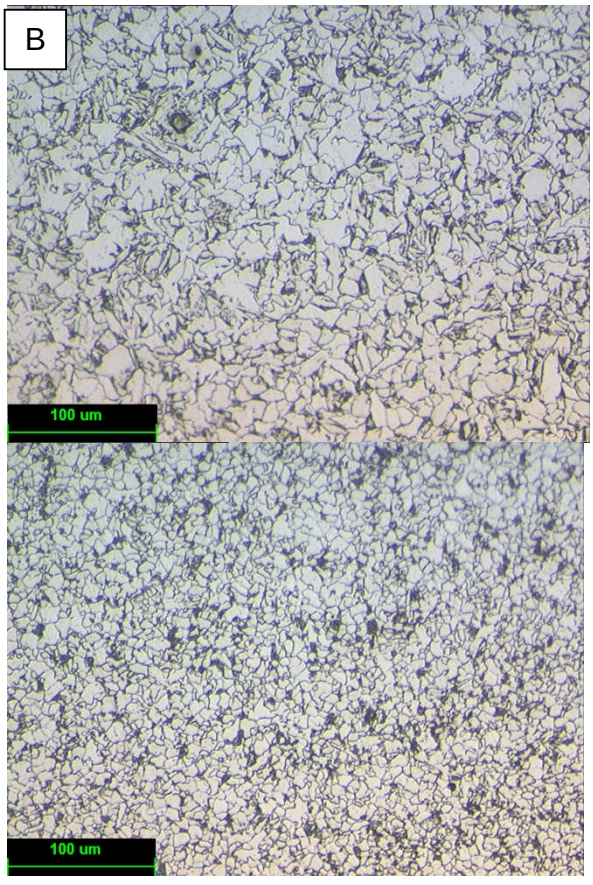
B
100 um
100 um

C

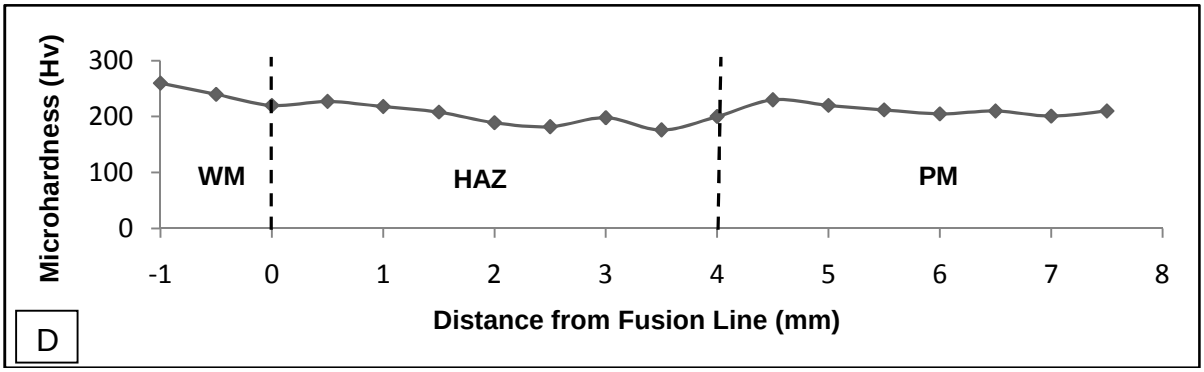

Figure 3 Microstructures of [A] fusion region of the weld, [B] fine grained HAZ and [C] parent material. D is the corresponding microhardness profile.

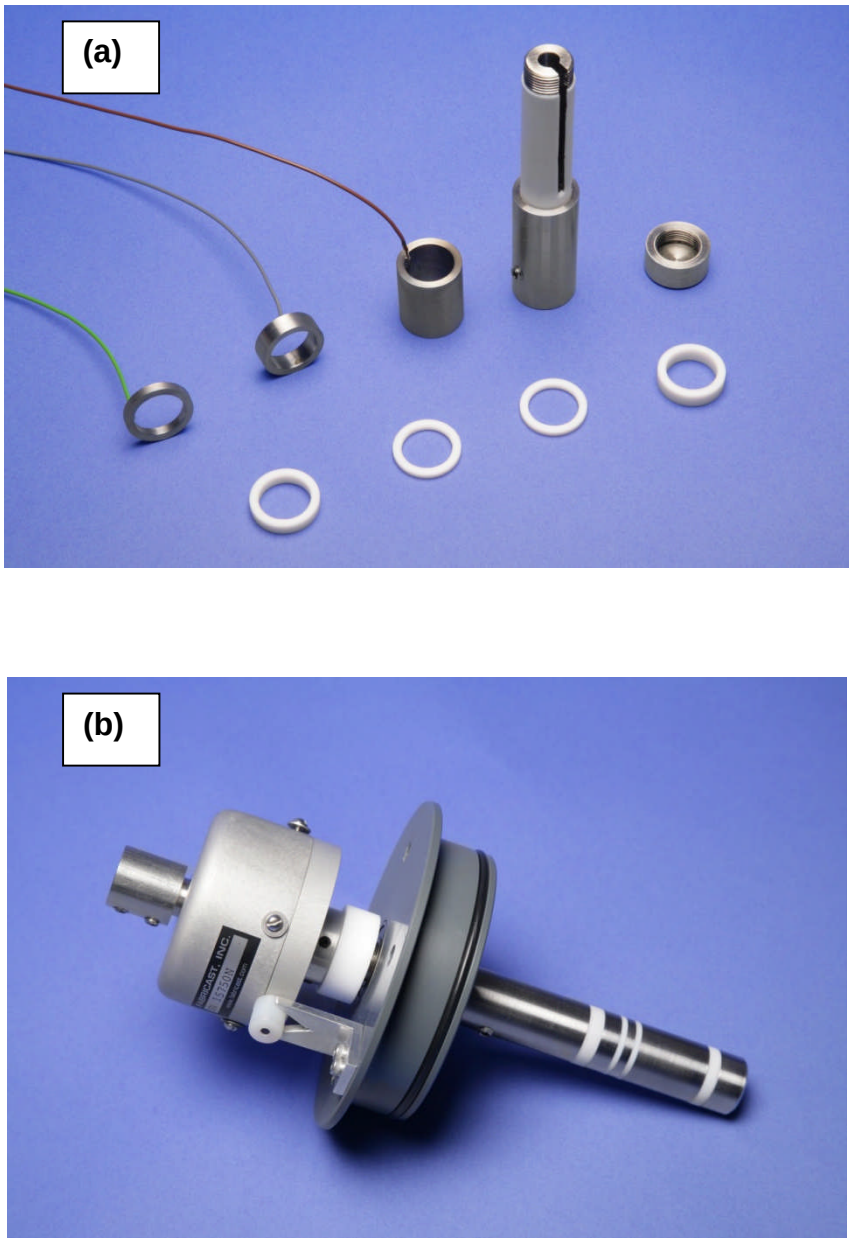

Figure 4 **The rotating cylinder electrode showing (a) the component parts (b) the complete assembly**

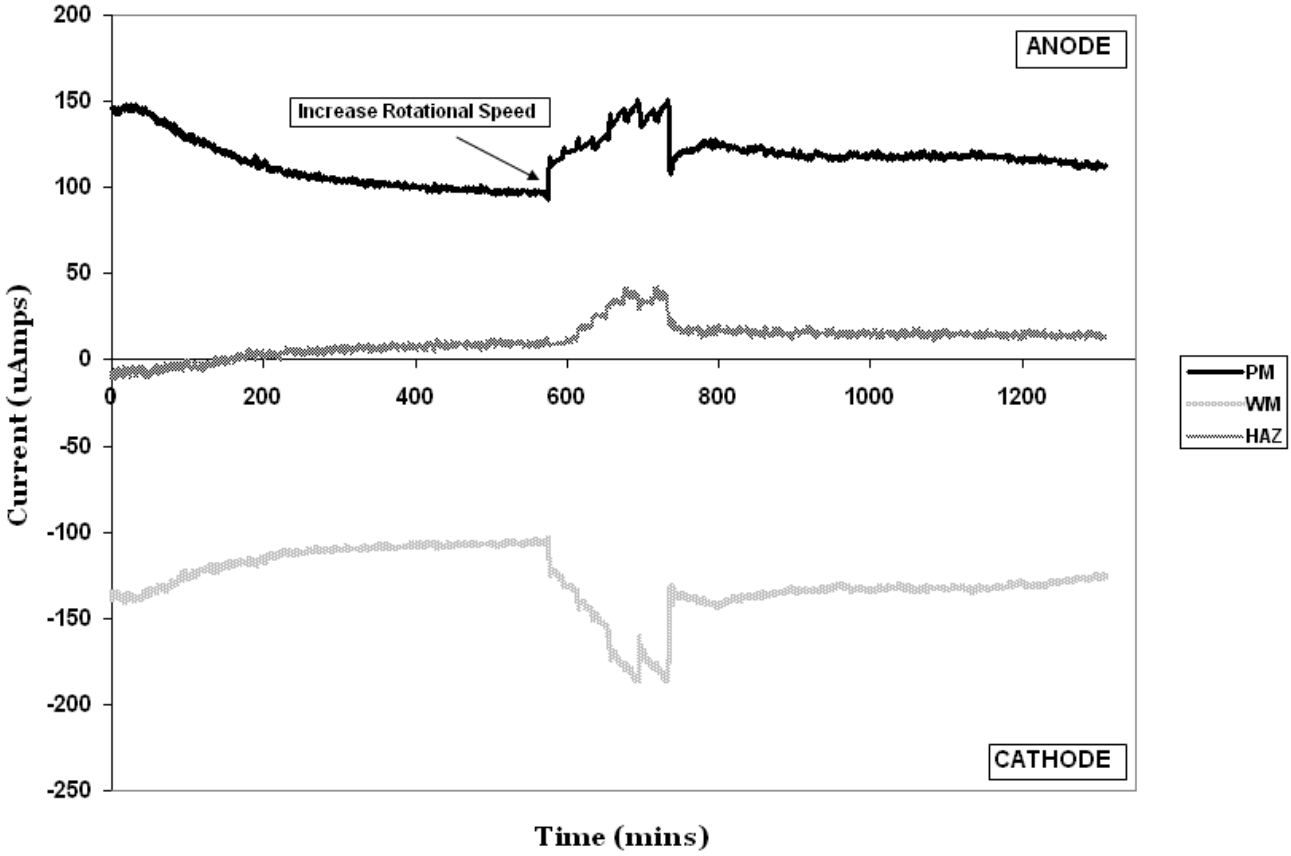

Figure 5 **Galvanic current measurements at ambient temperature without inhibitor showing sacrificial protection of the weld metal**

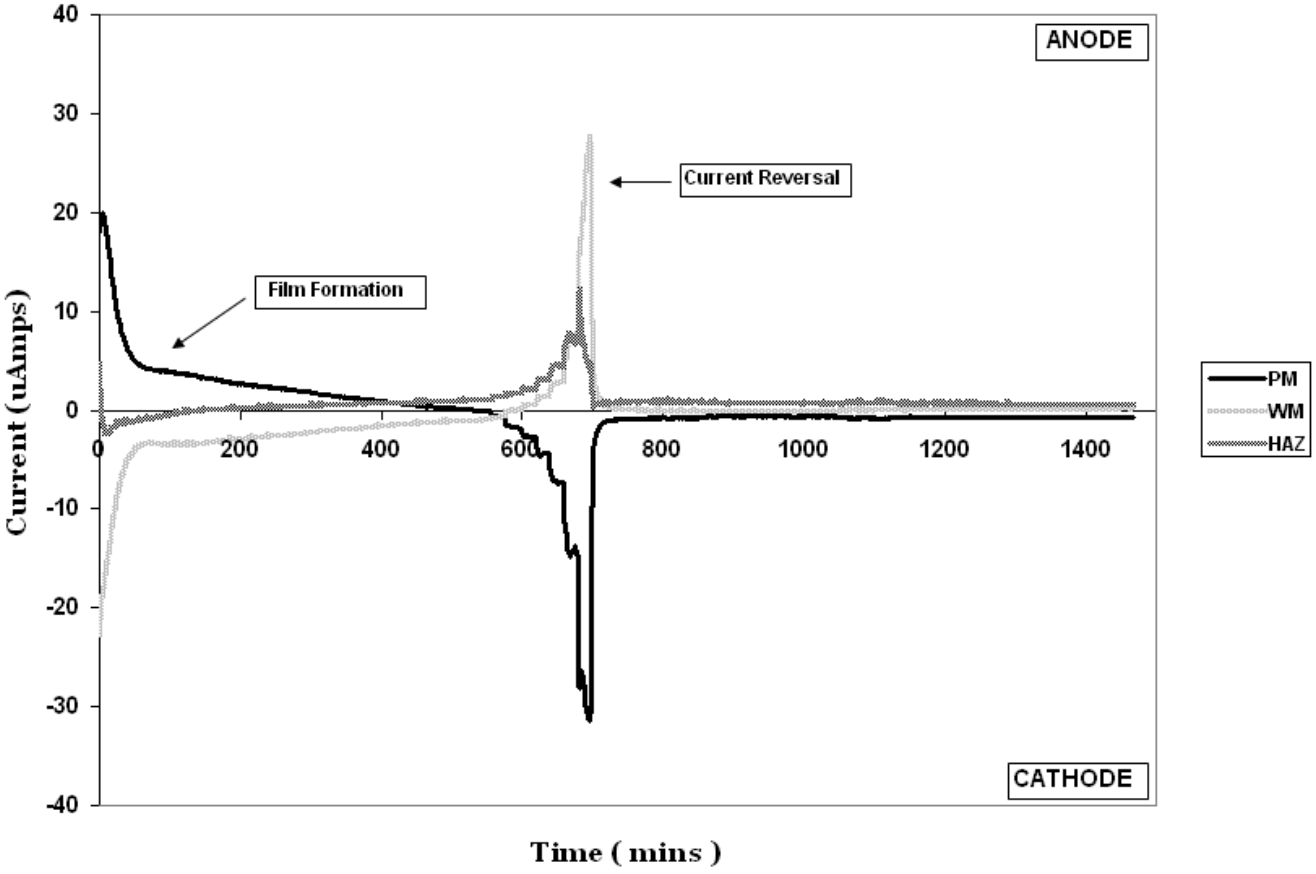

Figure 6 **Galvanic current measurements with inhibitor at ambient temperature showing current reversal and preferential corrosion of the weld metal**

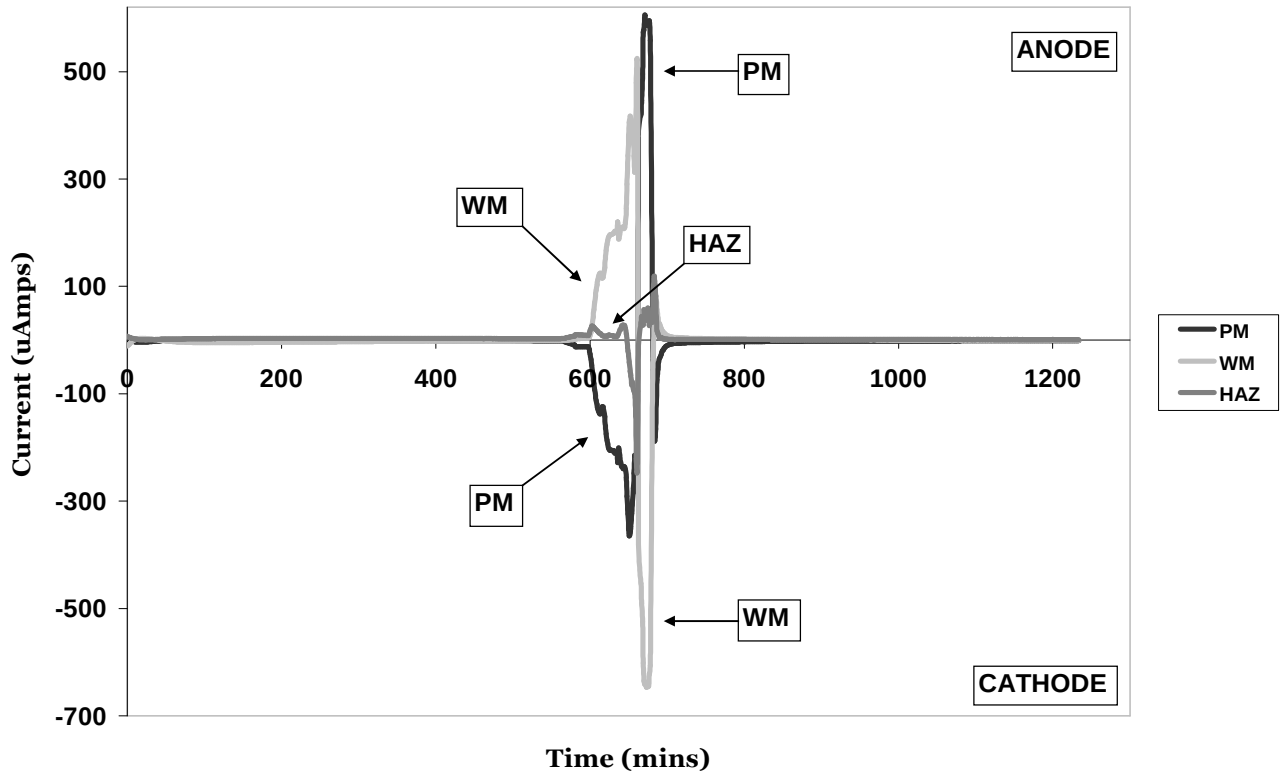

Figure 7 **Galvanic current measurements with inhibitor at ambient temperature showing a second current reversal at 5000 rpm**

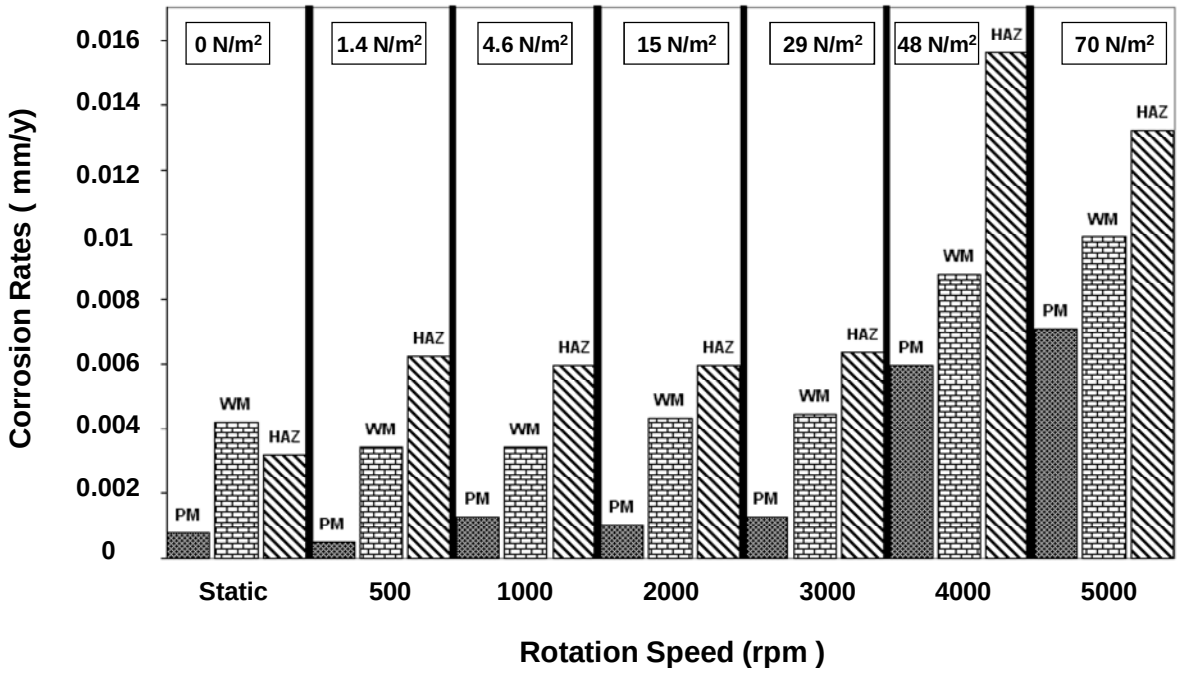

Figure 8 Self corrosion rates with inhibitor at ambient temperature

(a)

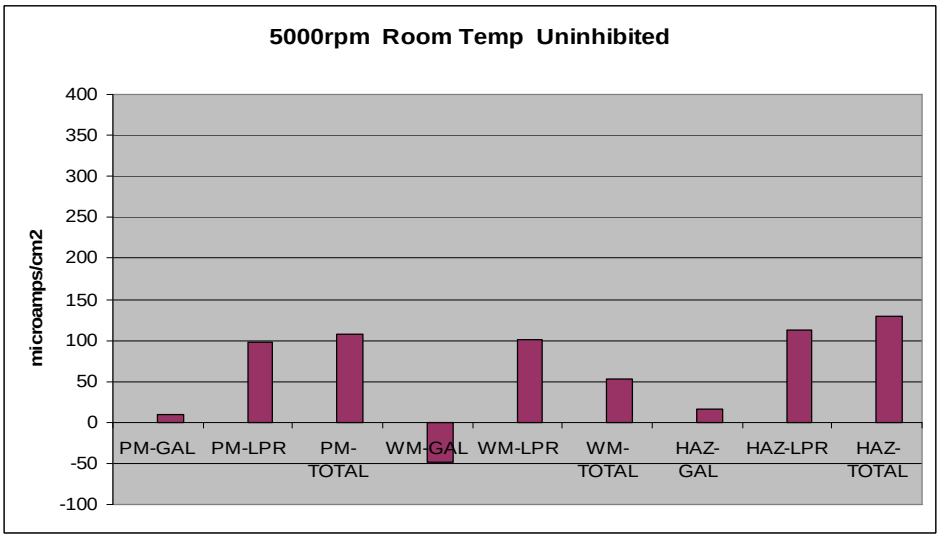

(b)

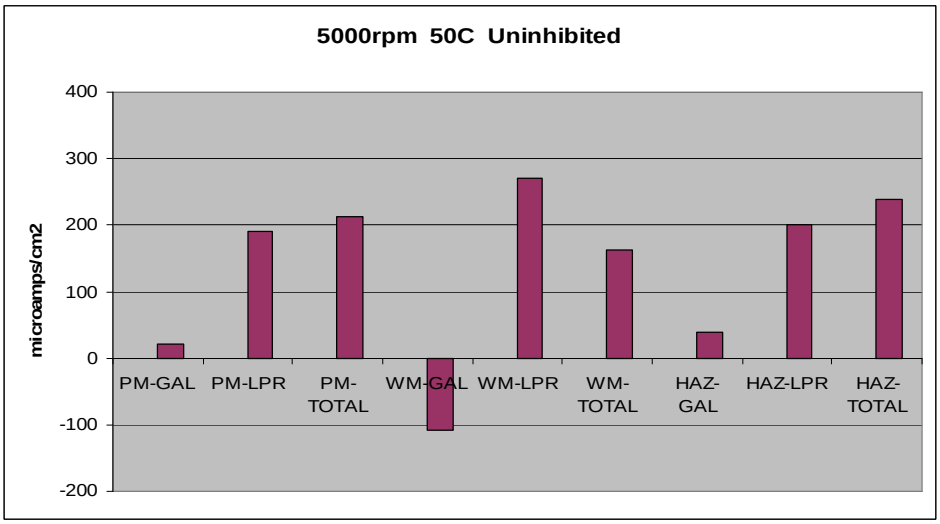

(c)

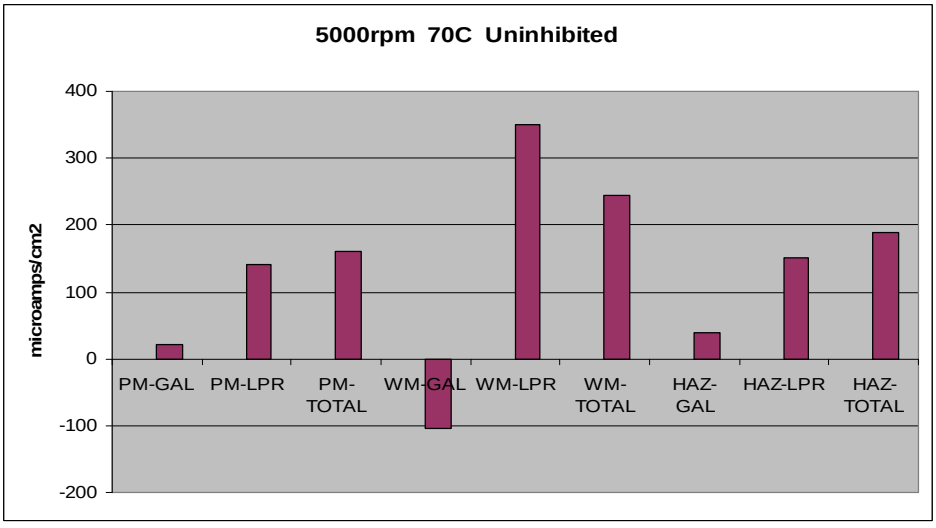

Figure 9 **Galvanic (GAL), self-corrosion (LPR) and total corrosion currents for each weld region in uninhibited conditions at 5000 rpm**

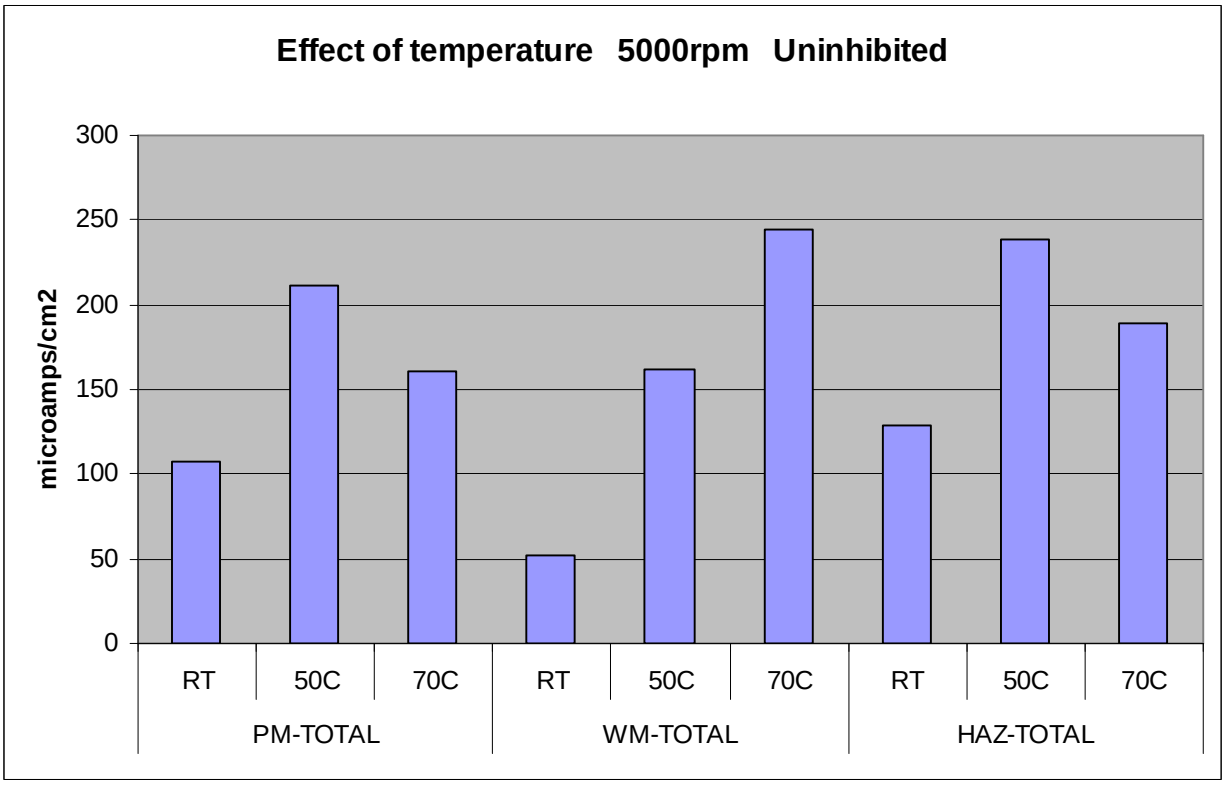

Figure 10 Total corrosion current densities in uninhibited conditions at 5000 rpm for each weld region showing the effects of test temperature

(a)

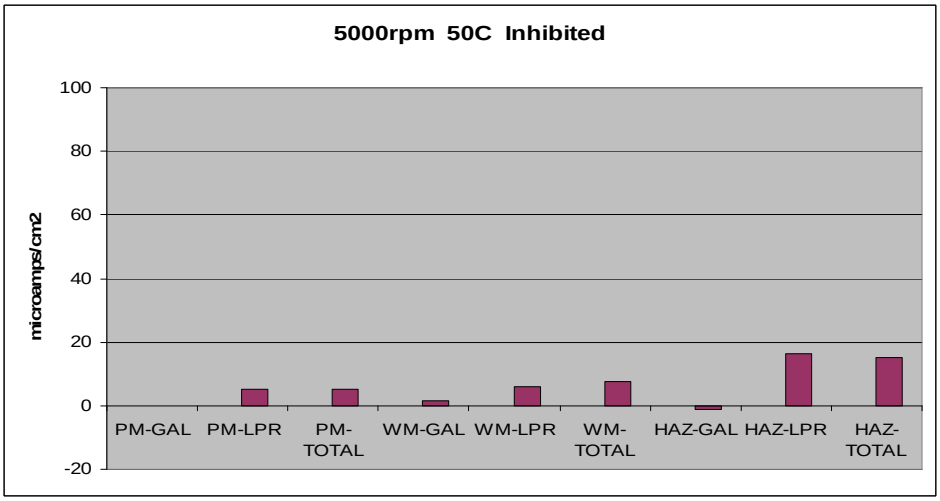

(b)

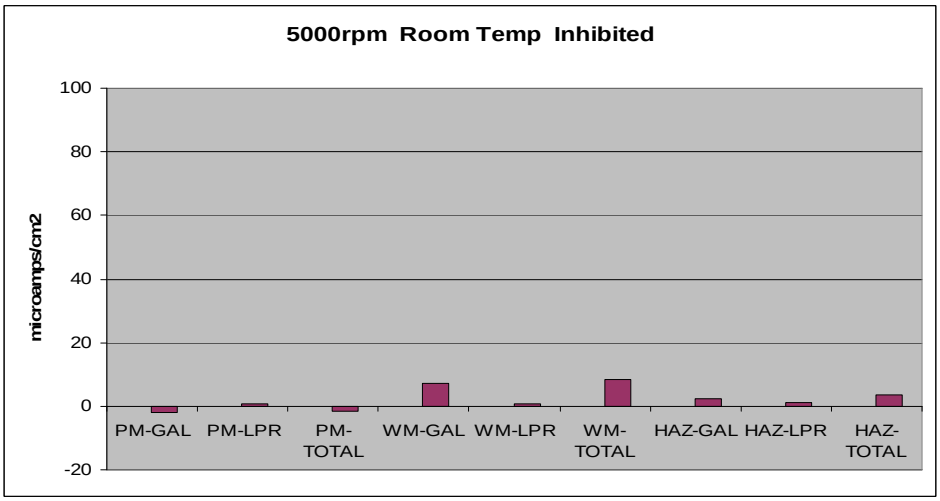

(c)

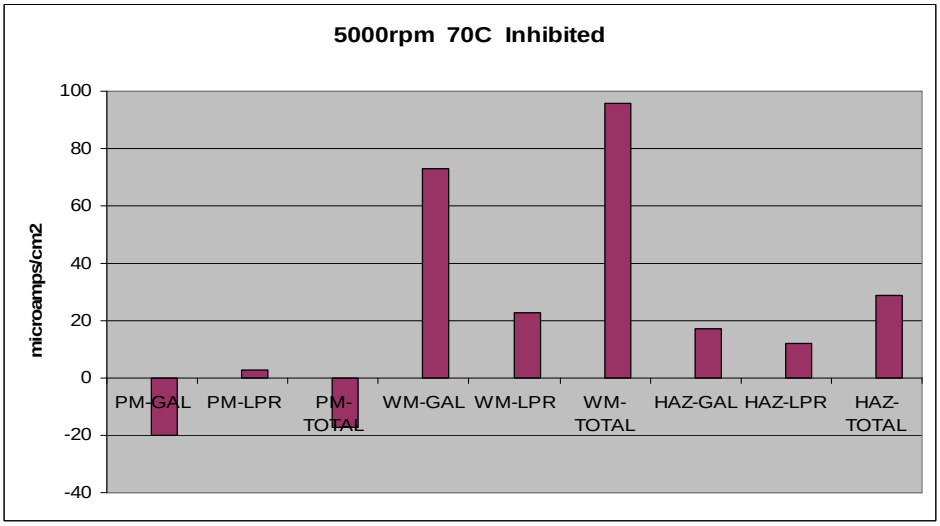

Figure 11 Galvanic (GAL), self-corrosion (LPR) and total corrosion currents for each weld region in inhibited conditions at 5000 rpm

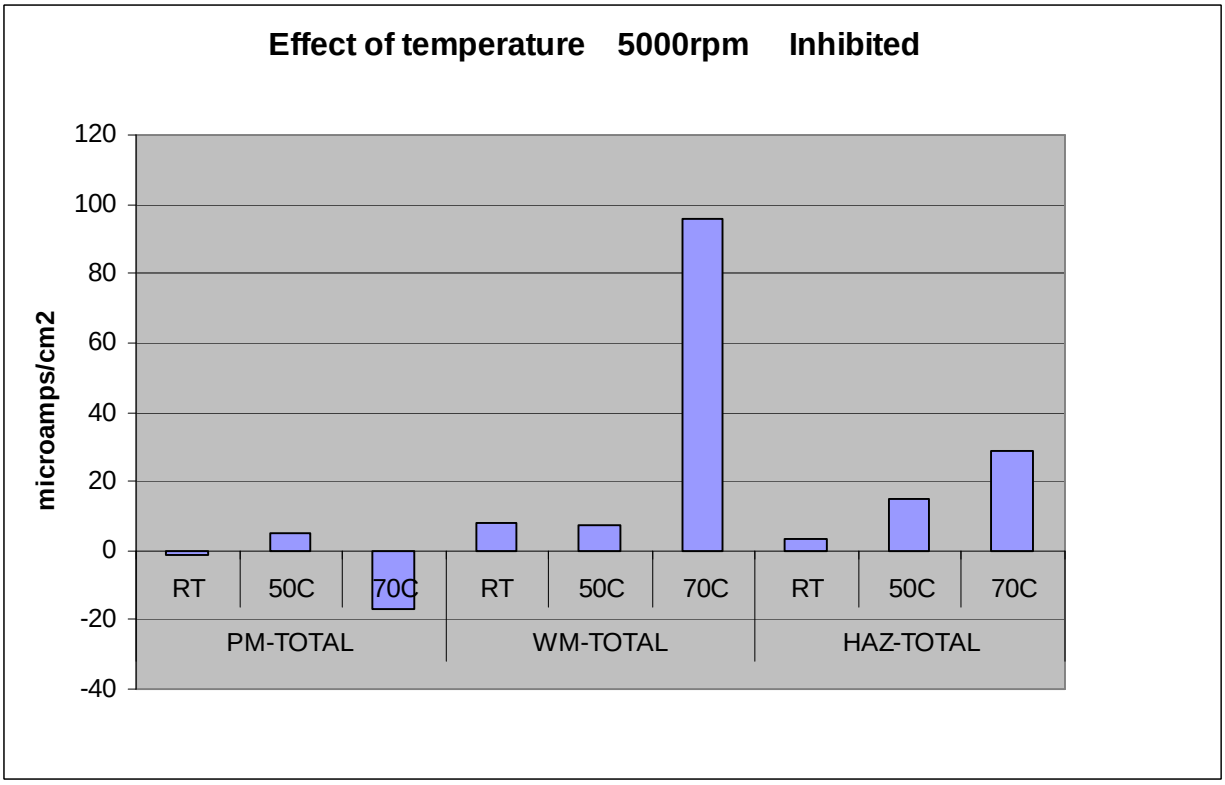

Figure 12 **Total corrosion current densities in inhibited conditions at 5000 rpm for each weld region showing the effects of test temperature**

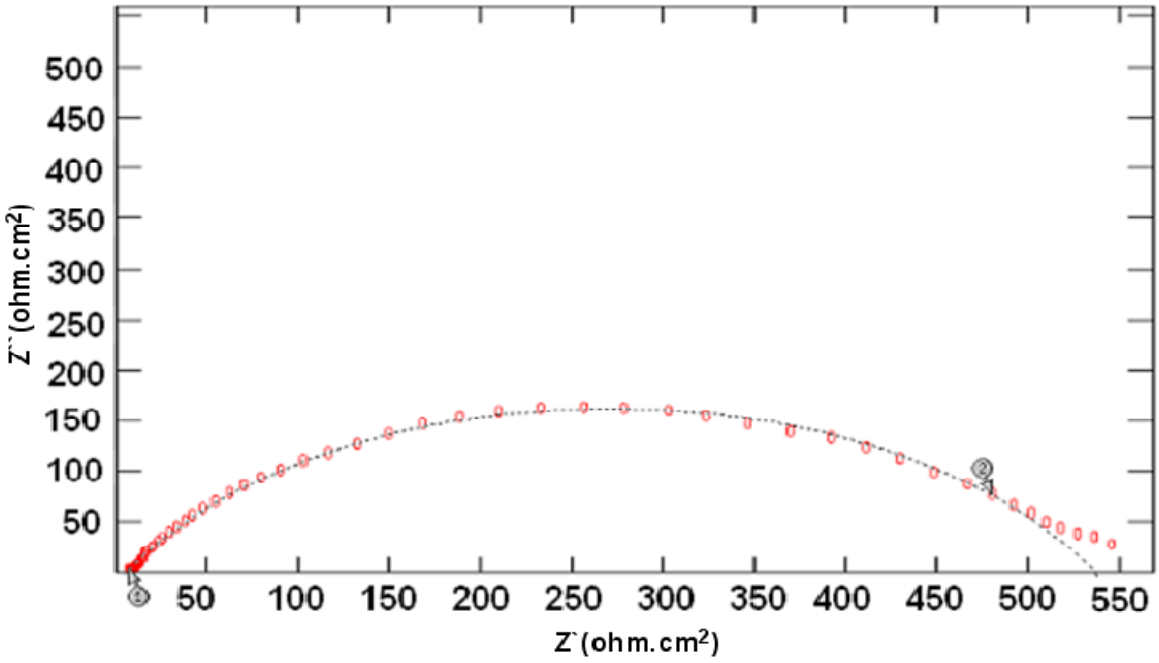

Figure 13 **Nyquist plot for parent material upon initial immersion in static, uninhibited conditions at ambient temperature**

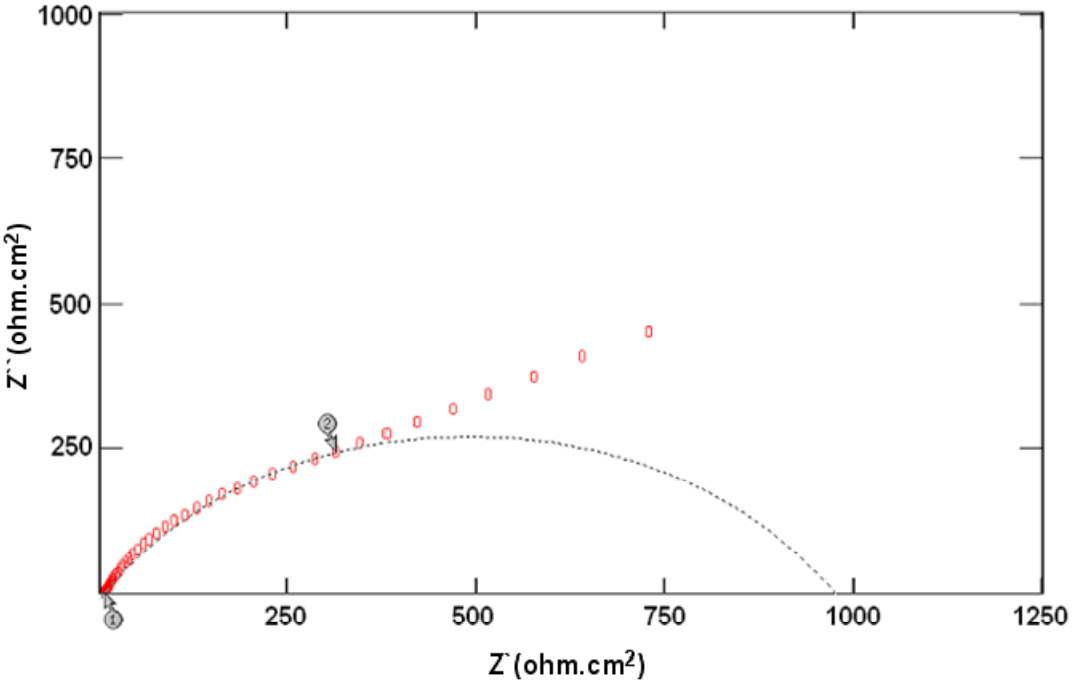

Figure 14 **Nyquist plot for parent material after 10h immersion in static, uninhibited conditions at ambient temperature**

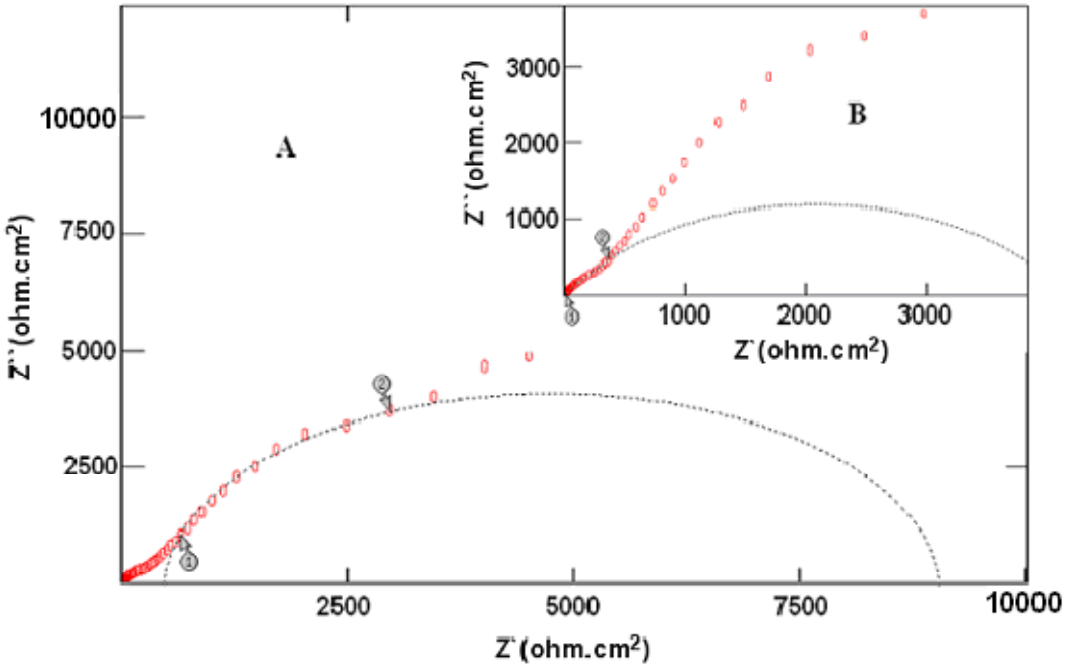

Figure 15 **(A) Nyquist plot for parent material after 10h immersion in inhibited conditions at 50°C and a rotational speed of 5000 rpm. (B) The response of the inhibitor film shown by the high frequency data**

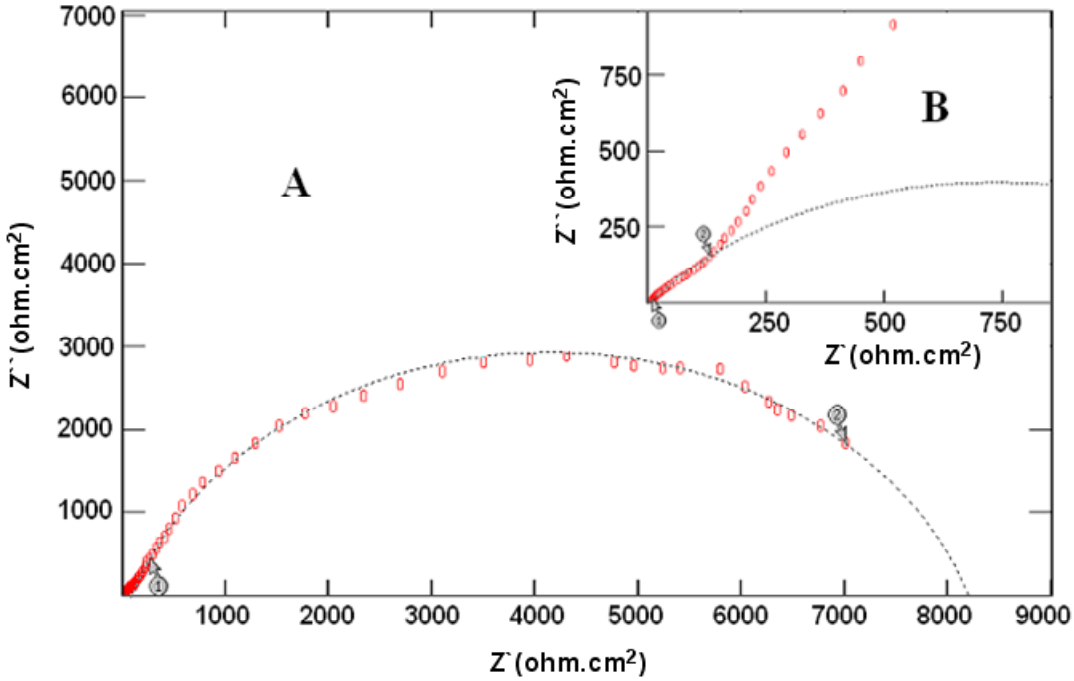

Figure 16 **(A) Nyquist plot for parent material after 10h immersion in inhibited conditions at 70°C and a rotational speed of 5000 rpm. (B) The response of the inhibitor film shown by the high frequency data**

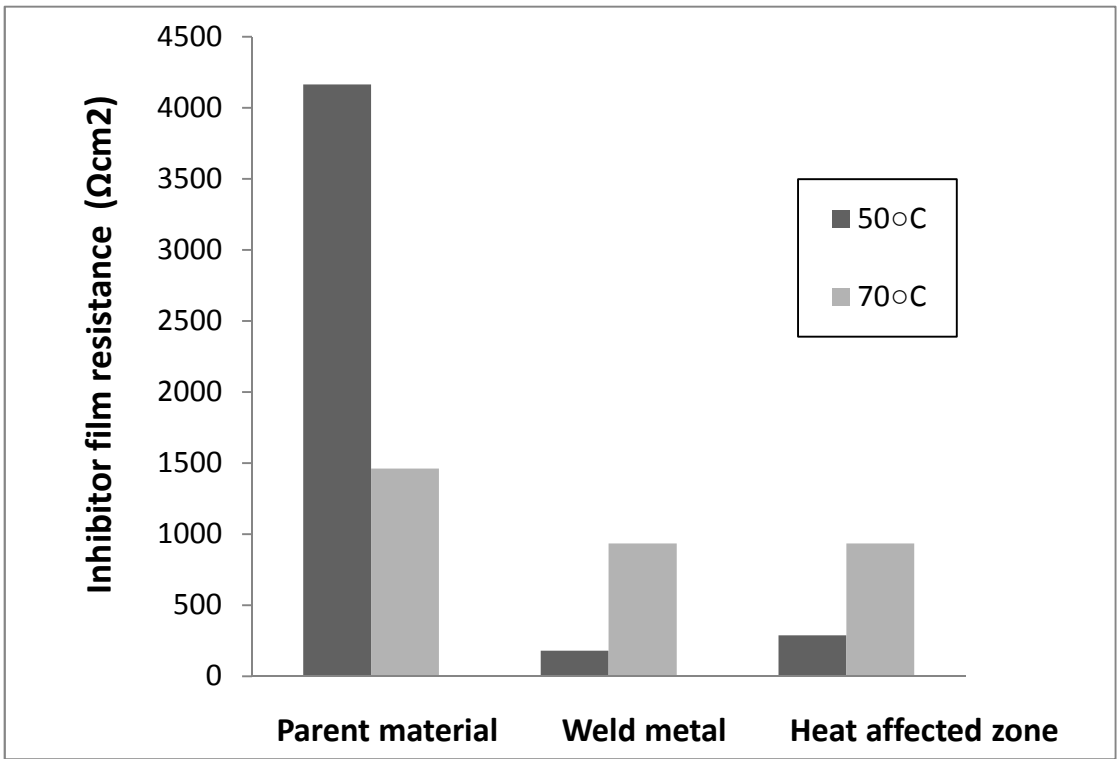

Figure 17 Comparison of inhibitor film resistance at 50°C and 70°C for each weld region measured in inhibited conditions at 5000 rpm

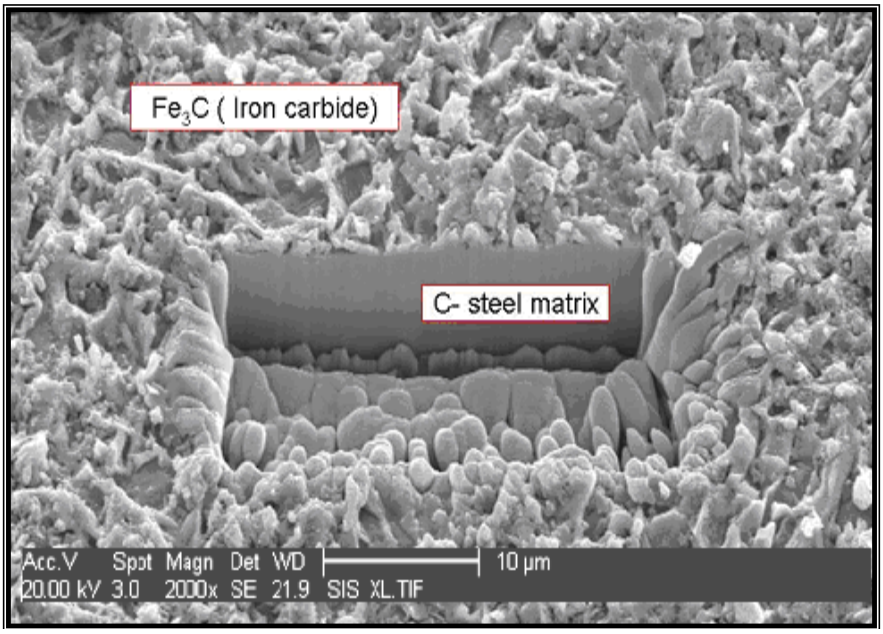

Figure 18 **SEM micrograph of the surface of the weld metal after 5 days in uninhibited conditions at 70°C showing the porous nature of the iron carbide network. The surface has been etched using FIB to reveal the cross-section**